

Theory of second harmonic generation in colloidal crystals

Y. C. Jian, C. Z. Fan, J. P. Huang*

*Surface Physics Laboratory and Department of Physics,
Fudan University, Shanghai 200433, China*

K. W. Yu

*Department of Physics and Institute of Theoretical Physics,
The Chinese University of Hong Kong, Shatin, New Territories, Hong Kong*

(Dated: February 9, 2020)

Abstract

Based on the Edward-Kornfeld formulation, we study the effective susceptibility of second-harmonic generation (SHG) in colloidal crystals, which are made of graded metallodielectric nanoparticles with an intrinsic SHG susceptibility suspended in a host fluid. We find a large enhancement and redshift of SHG responses, which arises from the periodic structure, local field effects and gradation in the metallic cores. The optimization of the Ewald-Kornfeld formulation is also investigated.

* Electronic address: jphuang@fudan.edu.cn

I. INTRODUCTION

In recent years, nonlinear composite materials with high nonlinear optical susceptibilities or optimal figure of merit (FOM) have drawn considerable attention for its potential applications, e.g., in bistable switches, optical correlators, and so on [1, 2, 3, 4, 5, 6]. With the advancements in nanotechnology, such as templated sedimentation and dielectrophoresis [7, 8, 9, 10], it is possible to fabricate particles with specific geometry. It has been reported [4, 6, 11, 12, 13] that graded composite materials whose physical properties vary gradually in space [14, 15] show enhanced nonlinear optical responses.

Materials lacking inversion symmetry can exhibit a so-called second order nonlinearity [1]. This can give rise to the phenomenon of second harmonic generation (SHG), i.e., an input (pump) wave can generate another wave with twice the optical frequency (namely, half the wavelength) in the medium. In most cases, the pump wave is delivered in the form of a laser beam, and the second-harmonic wave is generated in the form of a beam propagating in a similar direction. The physical mechanism behind SHG can be understood as follows. Due to the second order nonlinearity, the fundamental (pump) wave generates a nonlinear polarization which oscillates with twice the fundamental frequency. According to Maxwell's equations, this nonlinear polarization radiates an electromagnetic field with this doubled frequency. Due to phase matching issues, the generated second-harmonic field propagates dominantly in the direction of the nonlinear polarization wave. The latter also interacts with the fundamental wave, so that the pump wave can be attenuated (pump depletion) when the second-harmonic intensity develops. In the mean time, the energy is transferred from the pump wave to the second-harmonic wave. The SHG effect, like the third-order Kerr-type coefficient, involves the nonlinear susceptibilities of the constituents and local field enhancement which arises from the structure of composite materials. For example, Hui *et al.* studied a dilute suspension of coated particles with the shell having a nonlinear susceptibility for SHG [16], and two of us designed a class of ferrofluid-based soft nonlinear optical materials with enhanced SHG with magnetic-field controllabilities [17]. SHG and phase transformation behaviors can be detected in many nanocrystals by using classical ways like X-ray diffraction or Raman spectroscopy [18]. Until now, achieving enhanced SHG is a challenge [19, 20].

Theoretical [21] and experimental [22, 23] reports also suggested that spherical particles exhibit a rather unexpected and nontrivial SHG due to the broken inversion symmetry at particle surfaces (namely, atoms in the surface occupy positions that lack inversion symmetry), despite their central

symmetry which seemingly prohibits second-order nonlinear effects. In colloidal suspensions, the SHG response for centrosymmetric particles was experimentally reported [22, 23]. Most recently, SHG was also shown to appear for spherical semiconductor nanocrystals [24]. So far, the SHG from centrosymmetrical structure has received an extensive attention [21, 22, 23, 25, 26].

Colloidal crystals have been widely studied in nanomaterials and have potential applications in nanophotonics, chemistry, and biomedicine [27]. For colloidal crystals, the individual colloidal nanoparticles should be touching. As a matter of fact, it is possible to achieve a colloidal crystal without the particles' touching if the colloidal nanoparticles are charged and stabilized by electrostatic forces. In this work, we shall investigate colloidal crystals with the particles' touching. Owing to recent advancements in the fabrication of nanoshells [28, 29], we are allowed to use a dielectric surface layer with thickness d on a graded metallic core with radius a , in order to activate repulsive or attractive forces between the nanoparticles. The dielectric constant of the metallic core should be a radial function because of a radial gradation, and that of the surface layer can be the same as that of the host fluid, as to be used in this work. The latter is also a crucial requirement because otherwise multipolar interaction between the metallic cores can become important [30, 31]. In this regard, the surface layer contributes to the geometric constraint, rather than the effective optical responses of the colloidal crystals. In this work, based on the Ewald-Kornfeld formulation [Eq. (7)] [32] and the nonlinear differential effective dipole approximation (NDEDA) method [Eq. (4)] [33, 34], we shall focus on the possibility of achieving such colloidal crystals with desired SHG signals.

This paper is organized as follows. In section II, we apply the Ewald-Kornfeld formulation to derive the local electric field in three typical structures of colloid crystals, and then perform the NDEDA method to extract the effective linear dielectric constant and nonlinear susceptibility for SHG. In Section III, we discuss the optimization of the Ewald-Kornfeld summation. Then, we numerically investigate the SHG under different conditions in Section IV, which is followed by a discussion and conclusion in Section V.

II. FORMALISM

Let us start by considering a graded metallic core with radius a (Fig. 1). When we take into account quadratic nonlinearities only, the local constitutive relation between the displacement field

$\mathbf{D}(r)$ and electric field $\mathbf{E}(r)$ is given by [35, 36, 37]

$$D_i(r) = \sum_j \epsilon_{ij} E_j(r) + \sum_{jk} \chi_{ijk}(r) E_j(r) E_k(r), \quad i = x, y, z, \quad (1)$$

where $D_i(r)$ and $E_i(r)$ are the i th component of $\mathbf{D}(r)$ and $\mathbf{E}(r)$, respectively, and χ_{ijk} is the nonlinear susceptibility for SHG. Here $\epsilon_{ij} = \epsilon(r)\delta_{ij}$ denotes the linear dielectric constant, which is assumed for simplicity to be isotropic. Both $\epsilon(r)$ and $\chi_{ijk}(r)$ are functions of r , as a result of the gradation profile along the radius r (Fig. 1). If a monochromatic external field is applied, the nonlinearity in the system will generally generate local potentials and fields at all harmonic frequencies. For a finite frequency external electric field of the form

$$E_0 = E_0(\omega)e^{-i\omega t} + c.c., \quad (2)$$

the effective SHG susceptibility $\chi_{2\omega}$ can be extracted by considering the volume average of the displacement field at the frequency 2ω in the inhomogeneous medium [13, 16, 35, 36, 37]. The graded metallic core can be built up by adding shells gradually, making the dielectric constant $\epsilon_1(r)$ ($r \leq a$) a radial function, which is schematically shown in Fig. 1. We assume that the dielectric constant of the surface and the linear host fluid is a constant for convenience, as mentioned in Section I. At radius r , the inhomogeneous spherical particle with $\epsilon(r)$ and $\chi_{2\omega}(r)$ can have the same dipole moment effect as the homogenous sphere with $\bar{\epsilon}(r)$ and $\bar{\chi}_{2\omega}(r)$. The equivalent dielectric constant $\bar{\epsilon}(r)$ can be expressed as the following differential equation obtained from the differential effective dipole approximation method [14, 33],

$$\frac{d\bar{\epsilon}(r)}{dr} = \frac{(\bar{\epsilon}(r) - \epsilon(r))(\bar{\epsilon}(r) + 2\epsilon(r))}{r\epsilon(r)}. \quad (3)$$

On the other hand, the equivalent susceptibility for SHG $\bar{\chi}_{2\omega}(r)$ can be written as [34]

$$\begin{aligned} \frac{d\bar{\chi}_{2\omega}(r)}{dr} = & \bar{\chi}_{2\omega}(r) \left(\frac{2d\bar{\epsilon}_\omega(r)/dr}{2\epsilon_2 + \bar{\epsilon}_\omega(r)} + \frac{d\bar{\epsilon}_{2\omega}(r)/dr}{2\epsilon_2 + \bar{\epsilon}_{2\omega}(r)} + \frac{2y(\omega, r) + y(2\omega, r) - 3}{r} \right. \\ & \left. + 3 \frac{[x^2(\omega, r)(r) + \frac{28}{35}z^2(\omega, r)(r)]x(2\omega, r) + \frac{8}{35}[7x(\omega, r) + 2z(\omega, r)]z(\omega, r)z(2\omega, r)(r)}{r f(2\omega, r) f^2(\omega, r)(r)} \right), \end{aligned} \quad (4)$$

where $x(\omega, r) = \frac{\epsilon_2(r)(\bar{\epsilon}_\omega(r) + 2\epsilon_\omega(r))}{\epsilon_\omega(r)(\bar{\epsilon}_\omega(r) + 2\epsilon_2(r))}$, $y(\omega, r) = 2 \frac{(\bar{\epsilon}_\omega(r) - \epsilon_\omega(r))(\epsilon_\omega(r) - \epsilon_2(r))}{\epsilon_\omega(r)(\bar{\epsilon}_\omega(r) + 2\epsilon_2(r))}$, $z(\omega, r) = \frac{\epsilon_2(r)(\bar{\epsilon}_\omega(r) - \epsilon_\omega(r))}{\epsilon_\omega(r)(\bar{\epsilon}_\omega(r) + 2\epsilon_2(r))}$, and $f(\omega, r) = \frac{3\epsilon_2(r)}{\bar{\epsilon}_\omega(r) + 2\epsilon_2(r)}$. Here index ω and 2ω corresponds to basic and second harmonics for the nonlinear susceptibility, respectively, and $\bar{\chi}_{2\omega}(r)$ denotes the equivalent SHG susceptibility of the whole graded spherical particle with radius r . For convenience, we shall denote $\bar{\chi}_{2\omega}(r = a)$ as $\bar{\chi}_{2\omega}$ in the following.

The above two differential equations [Eqs. (3)-(4)] can be solved numerically as long as the gradation profiles are given. For obtaining the effective dielectric constant of the colloidal crystal, we refer to the Maxwell-Garnett formula [38, 39]

$$\frac{\epsilon_e - \epsilon_2}{\alpha\epsilon_e + (3 - \alpha)\epsilon_2} = \rho \frac{\bar{\epsilon} - \epsilon_2}{\bar{\epsilon} + 2\epsilon_2}, \quad (5)$$

where ρ denotes the volume fraction of the metallic component [see Eq. (6) below], and the local field factor α represents α_{\perp} (transverse field cases) and α_{\parallel} (longitudinal field cases), respectively. Here the longitudinal (or transverse) field case corresponds to the fact that the E field of the incident light is parallel (or perpendicular) to the uniaxial anisotropic axis. For α_{\perp} and α_{\parallel} , there is a sum rule $2\alpha_{\perp} + \alpha_{\parallel} = 3$ [40, 41]. Next, we shall apply the Ewald-Kornfeld model to compute the local field factor α for a tetragonal unit cell that can be viewed as a tetragonal lattice plus a basis of two nanoparticles. One of the two nanoparticles is located at the corner of the cell, and the other is at the body center. Without loss of generality, we consider three representative lattices (Fig. 2): the bct (body-centered tetragonal), bcc (body-centered cubic) and fcc (face-centered cubic) lattice. If the uniaxial anisotropic axis is directed along the z axis, the lattice constants can be denoted by $C_1(= C_2) = \ell q^{-\frac{1}{2}}$ along x (y) axis and $C_3 = \ell q$ along z axis, and the volume of the unit cell $V_c = \ell^3$. The lattice parameters satisfy the geometric constraint that $C_1^2 + C_2^2 + C_3^2 = 16(a + d)^2$, when we take into account the dielectric surface layer with thickness d on the graded metallic core. It is easy to obtain the value of q from their intrinsic structures: $q = 0.87358, 1.0$ and $2^{\frac{1}{3}}$ represent the bct, bcc and fcc lattice, respectively. Table I shows the calculated values of α_{\perp} and α_{\parallel} versus q , according to Eq. (7) below. The degree of anisotropy of the periodic lattices is measured by how q deviates from unity. Here we assume that the colloidal particles are packed closely together. Meanwhile, we obtain a relation between q and the volume fraction ρ of the metallic component,

$$\rho = \frac{\pi}{24t^3} \sqrt{\left(\frac{q^3 + 2}{q}\right)^3}, \quad (6)$$

with thickness parameter $t = (a + d)/a, t > 1$. The lattice vector of the tetragonal lattice is given by $\mathbf{R} = \ell(q^{-\frac{1}{2}}l\hat{x} + q^{-\frac{1}{2}}m\hat{y} + qn\hat{z})$, where l, m , and n are integers. When an external electric field \mathbf{E}_0 is applied along the x axis, the induced dipole moment \mathbf{p} are perpendicular to the uniaxial anisotropic axis. Considering the field contribution from all the other particles in the lattice, the local field \mathbf{E}_L at the lattice point $\mathbf{r} = \mathbf{0}$ can be given as

$$E_L = p \sum_{j=1}^2 \sum_{\mathbf{R} \neq \mathbf{0}} [-B(R_j) + x_j^2 q^2 C(R_j)] - \frac{4\pi p}{V_c} \sum_{\mathbf{G} \neq \mathbf{0}} \Theta(\mathbf{G}) \frac{G_x^2}{G^2} \exp\left(\frac{-G^2}{4\eta^2}\right) + \frac{4p\eta^3}{3\sqrt{\pi}}, \quad (7)$$

where $x_j = l - (j - 1)/2$, $R_j = |\mathbf{R} - (j - 1)(a\hat{\mathbf{x}} + b\hat{\mathbf{y}} + c\hat{\mathbf{z}})/2|$, and $\Theta(\mathbf{G}) = 1 + \exp[i(u + v + w)/\pi]$. In Eq. (7), B and C are two coefficients given in [41], $B(r) = \text{erfc}(\eta r)/r^3 + 2\eta/(\sqrt{\pi}r^2) \exp(-\eta^2 r^2)$ and $C(r) = 3\text{erfc}(\eta r)/r^5 + 4\eta^3/(\sqrt{\pi}r^2) + 6\eta/(\sqrt{\pi}r^4) \exp(-\eta^2 r^2)$, where $\text{erfc}(\eta r)$ is the complementary error function and η is an adjustable parameter making the summation converge rapidly. For details, please see the Appendix. \mathbf{G} denotes the reciprocal lattice vector of \mathbf{R} . Thus the local field factor in transverse fields can be defined as

$$\alpha_{\perp} = \frac{3}{4\pi} \frac{V_c E_L}{2p}. \quad (8)$$

For the bct, bcc and fcc lattices, we obtain $\alpha_{\perp} = 0.95351, 1.0$ and 1.0 , respectively. Following Refs. [16, 17], the effective SHG susceptibility of the whole system $\chi_{2\omega}$ is given by

$$\chi_{2\omega} = p\bar{\chi}_{2\omega}\Gamma(2\omega)(\Gamma(\omega))^2, \quad (9)$$

where $\Theta(\omega)$ denotes the factor in a linear system which, for consistency with Eq. (5) in getting ϵ_e , should also be determined by using the Maxwell-Garnett approach. Thus, we obtain

$$\Gamma(\omega) = \frac{3\epsilon_2}{(1 - p\alpha)\bar{\epsilon}(\omega) + (2 + p\alpha)\epsilon_2}. \quad (10)$$

Meanwhile, $\bar{\chi}_{2\omega}$ can be obtained through the NDEDA method [Eq. (4)].

III. OPTIMIZATION OF THE EWALD-KORNFELD SUMMATION [EQ. (7)]

In Eq. (7), we see the adjustable parameter η dominates the accuracy and the efficiency of the Ewald-Kornfeld summation [41, 42]. An important aspect of the Ewald-Kornfeld summation is the tuning in the sense of speed at well controlled errors. It should be chosen carefully in order to make the summations both in the real space and the reciprocal lattices converge rapidly [41, 42, 43]. On the other hand, the r -space cutoff r_c and the k -space cutoff k_c are also difficult to be determined [41, 42, 43]. In this section, we shall analyze the role of these 3 parameters, especially on lattices depicted in Fig. 2. Similarly, it can also be applied to other lattice models.

In condensed matter physics, complex dielectrics should obey the famous sum rule $\beta_x + \beta_y + \beta_z = 4\pi$, where β_x , β_y , and β_z are the local field factors along x , y , and z axes, respectively [Eq. (11)]. We shall use this rule to estimate the accuracy of our algorithm.

First of all, let us investigate how the lattice parameters affect the accuracy of calculation. We test 4 lattices with $\{C_1 = 1, C_2 = 1, C_3 = 1, 5, 10\}$ and $\{C_1 = 10, C_2 = 10, C_3 = 10\}$ respectively. The cutoffs in the r - and k - spaces are fixed to 3 which means that we take summation

over 6 periods in each direction. By using the relation mentioned above, we have

$$\beta_i = \frac{E_{L,i}(\mathbf{p}_i)V_c}{2p_i} \equiv \frac{4\pi}{3}\alpha, \quad (11)$$

where the subscript i stands for Cartesian directions x , y , and z . Next, let us plot the result of the Ewald-Kornfeld summation vs splitting parameter in Fig. ???. The total local field factor $\beta_{total} = \beta_x + \beta_y + \beta_z$ is normalized by 4π . When $\{C_1 = C_2 = C_3 = 1\}$, there is a wide platform with η goes from 1 to 3. In this case, the correctness of our algorithm can be guaranteed by choosing η with any value within the platform region. However, as C_3 increases, the anisotropic degree becomes strong, and the original platform rapidly shortens. In the lattice $\{C_1 = C_2 = 1, C_3 = 5\}$, the proper region of η only has the width 0.25. Further, in the lattice $\{C_1 = C_2 = 1, C_3 = 10\}$, the platform even disappears. At that time, the correct result could not be achieved if we would not adjust r_c and k_c . Another isotropic lattice $\{C_1 = C_2 = C_3 = 10\}$ is also investigated. Although the shape of the figure is similar with that of $\{C_1 = C_2 = C_3 = 1\}$, the platform is remarkably shrunk.

Next, let us see how the shape of summation region affects the accuracy. For highly anisotropic lattices, i.e. $\{C_1 = C_2 = 1, C_3 = 10\}$, the method of cubic region summation is not applicable because it counts in many source sites far from the field point along the uniaxial direction, but ignores many sites near the field point in the other two isotropic direction (see Fig. ???). It may be improved by using a spherical region summation. Set l , m , and n to be sum indices in r -space, and u , v , and w to be in k -space. For the cubic region summation, we just require all these indices should be within [-maximum, maximum]. But for the spherical region summation, the requirement turns out to be

$$(al)^2 + (bm)^2 + (cn)^2 \leq R_r^2, \quad (12)$$

$$(u/a)^2 + (v/b)^2 + (w/c)^2 \leq R_k^2 \quad (13)$$

Figure ??? shows the effect of such spherical region summation. The circle line is obtained by imposing the restriction that all summation indices are within [-5,5], and the star line is obtained by using the spherical region summation. The maximum radii, R_r [Eq. (12)] and R_k [Eq. (13)], are the length of the diagonal of the unit cell in r - and k -space, respectively,

$$(al)^2 + (bm)^2 + (cn)^2 \leq a^2 + b^2 + c^2 = R_r^2, \quad (14)$$

$$(u/a)^2 + (v/b)^2 + (w/c)^2 \leq (1/a)^2 + (1/b)^2 + (1/c)^2 = R_k^2. \quad (15)$$

This summation region is smaller than the cubic region, and less sites are evaluated naturally. Nevertheless, a wider platform is achieved for this region. The main reason is that the spherical region summation tends to count in the sites which contribute much to the field point. The two lines in Fig. ?? show the same value when η becomes larger. Later we shall see that this is because of the result in the k -space summation that is not modified too much.

Last, we demonstrate how r_c and k_c affect the accuracy. In general, the larger radii the cutoff has, the more precise the result is. Unfortunately, larger summation regions cost longer computational time. Thus, we should take optimized values of r_c and k_c . In Fig. ??, we calculate the total local field factor for four configurations of cutoffs. The left-top graph is copied from Fig. ?. Meanwhile, the right-bottom plot is obtained with twice value of r_c and k_c . We can find that by increasing r_c , the platform would extend to the left with the limit of zero, but there is no such limit by increasing k_c . As k_c increases, the platform could extend to the wide space on the right.

In conclusion, in order to optimize the Ewald-Kornfeld summation, we should carry out the sum in a spherical shape. Enlarging the summation radius in k -space is more efficient than that in r -space. Our method might test the sum rule first with a large enough r_c and k_c (here time is not the main concern), and then it is convenient for one to choose the center value of η in the platform. This guarantees the correctness of all the computations performed for achieving Table I.

IV. NUMERICAL RESULTS

For numerical calculations, we set the linear dielectric constant of the nonlinear metallic core to have the following Drude form

$$\epsilon(r) = 1 - \frac{\omega_p(r)^2}{\omega(\omega + i\gamma)}, \quad (16)$$

where $\omega_p(r)$ means a position-dependent plasma frequency, and γ relaxation rate. For achieving the position-dependent plasma frequency, one possible way is to fabricate metallic spherical particles containing multilayers each of which is made of different metals. For numerical calculations, we take a model plasma-frequency gradation profile

$$\omega_p(r) = \omega_p(0) \left(1 - C_\omega \frac{r}{a}\right), \quad (17)$$

where C_ω is a parameter adjusting the gradation profile. For focusing on the enhancement of the SHG response, we take the intrinsic nonlinear SHG susceptibility χ_1 to be a frequency-and-position independent real positive constant.

Figure 3 shows the (a) imaginary part of the effective linear dielectric constant (namely, optical absorption), the (b) real and (c) imaginary parts of the effective SHG susceptibility, the (d) modulus of $\bar{\chi}_{2\omega}/\chi_1$, and the (e) FOM (figure of merit) versus the function of frequency for longitudinal field cases. The strength of the nonlinear polarization of nonlinear materials is reflected by the magnitude of the high-order harmonics. As C_ω increases, $\omega_p(r)$ takes on a broader range of value and leads to a broad plasmon band, while the plasmon peak redshifts to lower frequencies. The susceptibility of the SHG also shows an enhancement and the peak of enhancement can be shifted to lower frequencies, too. Generally, the SHG susceptibility and FOM can be enhanced in some regions as C_ω increases.

Figure 4 shows the effective responses and FOM as a function of thickness parameter t , for bct lattices. For the given lattice it is evident that the effective linear and nonlinear optical responses strongly depend on the thickness parameter. Both the redshift and strength of the plasma resonant peak or band are largest at the smallest t for linear optical absorption. This is the combination of gradation, local fields, and periodic lattice effects. In fact, the volume fraction for different colloidal lattices also contributes to the nature of plasma resonant. For the fcc lattice, the redshift lies between bct and bcc lattice, but they have only slight difference (no pictures shown here). This structure transformation can be detected in experiment. It can also be found that as t increases (or, alternatively the colloid crystal becomes more dilute), the behavior of plasma resonant becomes more similar. This can be explained from the dilute limit approximation model for the enhancement of optical susceptibility.

In Figs. 3 and 4 the quantities that can be both positive and negative are plotted in a logarithm of modulus. When the quantities pass through zero, the logarithm is very large, thus yielding spikes. In addition, we can reach the conclusion that the FOM in the high frequency region is still attractive due to the presence of weak optical absorption.

V. DISCUSSION AND CONCLUSION

As the value of q increases, the responses in transverse field will have slight difference from the longitudinal case (no figures shown here), because of the little difference between α_\perp and α_\parallel for a given structure. From bct, bcc to fcc lattices, with the increase of q , the longitudinal local field factor α_\parallel decreases from 1.09299 at bct lattice to 1.0 at bcc and fcc lattice, while the volume fraction p decreases to bct and bcc, then increases to fcc. This trend can also be seen in other bulk

samples, such as rhombohedral, orthorhombic and hexagonal.

We have investigated the cases of graded plasma frequencies, by assuming the relaxation rate γ to be a constant. In fact, γ can also be inhomogeneous. For instance, a position-dependent profile for the relaxation rate can be achieved experimentally. One possible way may be to fabricate dirty metallic spherical particles in which the degree of disorder varies in the radial direction and hence leads to a relaxation-rate gradation profile. In case of graded relaxation rates, the nonlinear optical responses can also be adjusted by choosing appropriate gradation profiles for relaxation rates [11].

Throughout the paper, the host medium is assumed to be isotropic. It is interesting to see what will happen if the host is anisotropic, e.g., for a graded-index host [44]. In this case, the gradation is also expected to yield desired enhanced SHG. On the other hand, optical switching in graded plasmonic crystals via nonlinear pumping was recently reported [45], which might also be realized in graded colloidal crystals proposed in this work.

In summary, we have theoretically exploited a class of nonlinear materials possessing a non-vanishing SHG susceptibility, which are based on colloidal crystals of graded metallodielectric nanoparticles. They have been shown to have an enhancement and redshift of SHG signals due to the combination of various effects.

Acknowledgments

Y.C.J. and J.P.H. acknowledge the financial support by the National Natural Science Foundation of China under Grant No. 10604014, by the Shanghai Education Committee and the Shanghai Education Development Foundation ("Shu Guang" project), and by the Pujiang Talent Project (No. 06PJ14006) of the Shanghai Science and Technology Committee. K.W.Y. acknowledges financial support through RGC Grant from the Hong Kong SAR Government. We are grateful to Professor P. M. Hui for fruitful discussion.

-
- [1] Y. R. Shen, *The Principles of Nonlinear Optics* (Wiley, New York, 1984).
- [2] R. W. Boyd, *Nonlinear Optics* (Academic, New York, 1992).
- [3] D. C. Rodenberger, J. R. Heflin, and A. F. Garito, *Nature (London)* **359**, 309 (1992).
- [4] G. L. Fischer, R. W. Boyd, R. J. Gehr, S. A. Jenekhe, J. A. Osaheni, J. E. Sipe, and L. A. Weller-Brophy, *Phys. Rev. Lett.* **74**, 1871 (1995).
- [5] T. Sekikawa, A. Kosuge, T. Kanai, and S. Watanabe, *Nature (London)* **432**, 605 (2004).
- [6] J. P. Huang and K. W. Yu, *Phys. Rep.* **431**, 87 (2006).
- [7] A. V. Blaaderen, *MRS Bull.* **29**, 85 (2004).
- [8] K. P. Velikov, C. G. Christova, R. P. A. Dullens, and A. Van Blaaderen, *Science* **296**, 106 (2002).
- [9] T. Gong and D. W. Marr, *Appl. Phys. Lett.* **85**, 3760 (2004).
- [10] T. Schilling, D. Frenkel, *Phys. Rev. Lett.* **92**, 085505 (2004).
- [11] J. P. Huang and K. W. Yu, *Appl. Phys. Lett.* **85**, 94 (2004).
- [12] R. S. Bennink, Y.-K. Yoon, R. W. Boyd, and J. E. Sipe, *Opt. Lett.* **24**, 1416 (1999).
- [13] J. P. Huang and K. W. Yu, *Opt. Lett.* **30**, 275 (2005).
- [14] G. W. Milton, *The Theory of Composites* (Cambridge University Press, Cambridge, 2002), Chap. 7.
- [15] C. Z. Fan, J. P. Huang, and K. W. Yu, *J. Phys. Chem. B* **110**, 25665 (2006).
- [16] P. M. Hui and D. Stroud, *J. Appl. Phys.* **82**, 4740 (1997).
- [17] C. Z. Fan and J. P. Huang, *Appl. Phys. Lett.* **89**, 141906 (2006).
- [18] H. P. Chiang, P. T. Leung and W. S. Tse, *J. Phys. Chem. B* **104**, 2348 (2000); J. Han, D. Chen, S. Ding, H. Zhou, Y. Han, G. Xiong, and Q. Wang, *J. Appl. Phys.* **99**, 023526 (2006).
- [19] D. Pezzetta, et al., *J. Opt. Soc. Am. b* **19**, 2102 (2002).
- [20] G. Purvinis, et al., *Opt. Lett.* **29**, 1108 (2004).
- [21] J. I. Dadap, J. Shan, K. B. Eisenthal, and T. F. Heinz, *Phys. Rev. Lett.* **83**, 4045 (1999).
- [22] N. Yang, W. E. Angerer, and A. G. Yodh, *Phys. Rev. Lett.* **87**, 103902 (2001).
- [23] S. H. Jen and H. L. Dai, *J. Phys. Chem. B* **110**, 23000 (2006).
- [24] D. H. Son, J. S. Wittenberg, U. Banin, and A. P. Alivisatos, *J. Phys. Chem. B* **110**, 19884 (2006).
- [25] P. Xu, S. H. Ji, S. N. Zhu, X. Q. Yu, J. Sun, H. T. Wang, J. L. He, Y. Y. Zhu, and N. B. Ming, *Phys. Rev. Lett.* **93**, 133904 (2004).
- [26] R. Bernal and J. A. Maytorena, *Phys. Rev. B* **70**, 125420 (2004).

- [27] *Colloids and Colloid Assemblies*, edited by F. Caruso (Wiley-VCH, Weinheim, 2004).
- [28] C. L. Nehl, N. K. Grady, G. P. Goodrich, F. Tam, N. J. Halas, and J. H. Hafner, *Nano Lett.* **4**, 2355 (2004).
- [29] D. B. Mitzi, L. L. Kosbar, C. E. Murray, M. Copel, and A. Afzali, *Nature (London)* **428**, 299 (2004).
- [30] J. P. Huang and K. W. Yu, *Appl. Phys. Lett.* **87**, 071103 (2005).
- [31] G. Q. Gu, K. W. Yu, and P. M. Hui, *J. Chem. Phys.* **116**, 10989 (2002).
- [32] P. P. Ewald, *Ann. Phys. (Leipzig)* **64**, 253 (1921); H. Kornfeld, *Z. Phys.* **22**, 27 (1924).
- [33] L. Gao, J. P. Huang, and K. W. Yu, *Phys. Rev. B* **69**, 075105 (2004), and references therein.
- [34] L. Gao and K. W. Yu, *Phys. Rev. B* **72**, 075111 (2005).
- [35] P. M. Hui, C. Xu, D. Stroud, *Phys. Rev. B* **69**, 014202 (2004).
- [36] P. M. Hui, C. Xu, D. Stroud, *Phys. Rev. B* **69**, 014203 (2004).
- [37] J. P. Huang, P. M. Hui, and K. W. Yu, *Phys. Lett. A* **342**, 484 (2005).
- [38] C. K. Lo, Jones T. K. Wan, and K. W. Yu, *J. Phys.: Condens. Matter* **13**, 1315 (2001).
- [39] J. P. Huang and K. W. Yu, *J. Chem. Phys.* **121**, 7526 (2004).
- [40] L. D. Landau, E. M. Lifshitz, and L. P. Pitaevskii, *Electrodynamics of Continuous Media*, 2nd ed. (Pergamon, New York, 1984), Chap. II.
- [41] C. K. Lo, and K. W. Yu, *Phys. Rev. E* **64**, 031501 (2001).
- [42] L. Shen, *Dynamic electrorheological effects of rotating spheres*, MPhil thesis, Chinese University of Hong Kong, Hong Kong, 2005.
- [43] Z. Wang and C. Holm, *J. Chem. Phys.* **115**, 6351 (2001).
- [44] J. J. Xiao and K. W. Yu, *Appl. Phys. Lett.* **88**, 071911 (2006).
- [45] J. J. Xiao, K. Yakubo and K. W. Yu, *Appl. Phys. Lett.* **88**, 241111 (2006).

TABLE I: Values of α_{\perp} and α_{\parallel} computed at different q . $q = 0.87358$, 1 , and $2^{1/3}$ correspond to bct, bcc, and fcc lattices, respectively.

q	α_{\perp}	α_{\parallel}
0.87358	0.953506	1.09299
0.9	0.971231	1.05754
1.0	1	1
1.1	0.999345	1.00131
1.2	0.996275	1.00745
$2^{1/3}$	1	1
1.3	1.00601	0.987988
1.4	1.03492	0.930155
1.5	1.08376	0.832478
1.6	1.15032	0.699352
1.7	1.23137	0.537268
1.8	1.32368	0.352638
1.9	1.42459	0.150817

Figure captions

Fig. 1. Schematic graph showing the graded metallic core with radius a embedded in a linear host fluid. The graded metallic core can be fabricated by adding shells gradually, which is aggrandized here. ϵ_2 denotes the linear dielectric constant of the host fluid, and $\epsilon(r)$ is the radius-dependent dielectric constant of the graded metallic core.

Fig. 2. Schematic graph showing unit cells of (a) bct, (b) bcc, and (c) fcc lattices.

Fig. 3. Normalized total local field factors versus splitting parameters in different lattices. η in the range of $\beta_{\text{total}}/(4\pi) = 1$ leads to accurate result of the Ewald-Kornfeld summation.

Fig. 4. Cubic and spherical summation region for lattices with different anisotropic degree.

Fig. 5. (Color online) Normalized total local field factors versus splitting parameters in cubic and spherical region summation. The platform for suitable η is widened by using spherical region summation.

Fig. 6. Normalized total local field factors versus splitting parameters for various r_c and k_c cutoffs. Increasing r_c or k_c yields the left or right extension of the platform, respectively.

Fig. 7. For the bct lattice (longitudinal field), (a) the linear optical absorption $\text{Im}[\epsilon_e(\omega)]$, (b) $\text{Im}[\chi_{2\omega}/\chi_1]$, (c) $\text{Re}[\chi_{2\omega}/\chi_1]$, (d) modulus of $\chi_{2\omega}/\chi_1$, and (e) the FOM= $|\chi_{2\omega}|/[\chi_1\text{Im}(\epsilon_e)]$ versus the normalized incident angular frequency of $\omega/\omega_p(0)$ for the dielectric function gradation profile [Eq. (16)] with various plasma-frequency gradation profiles [Eq. (17)]: $C_\omega = 0.3, 0.5, \text{ and } 0.7$. Here $|\dots|$ denotes the absolute value or modulus of \dots . Parameters: $\gamma = 0.02\omega_p(0)$, $t = 3$, and $\epsilon_2 = 2.25$.

Fig. 8. Same as Fig. 3, but for different thickness $t = 1.2, 2.0, \text{ and } 3.0$. Parameters: $\gamma = 0.02\omega_p(0)$, $C_\omega = 0.5$, and $\epsilon_2 = 2.25$.

FIG. 1: /Jian, Fan, Huang, and Yu

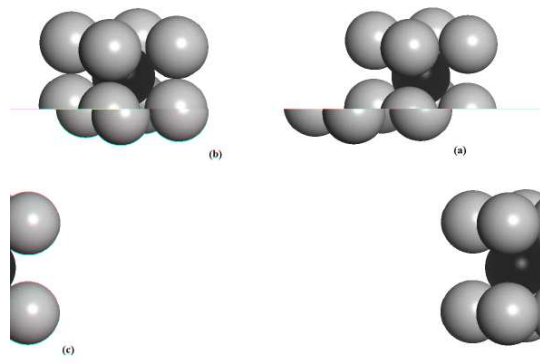


FIG. 2: /Jian, Fan, Huang, and Yu

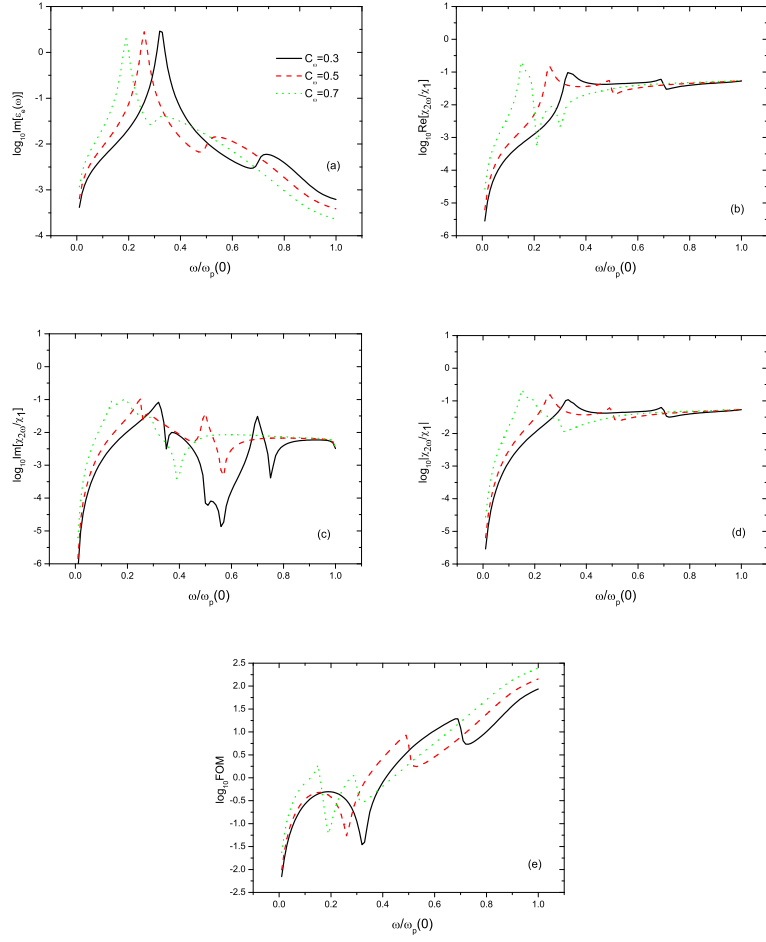


FIG. 3: /Jian, Fan, Huang, and Yu

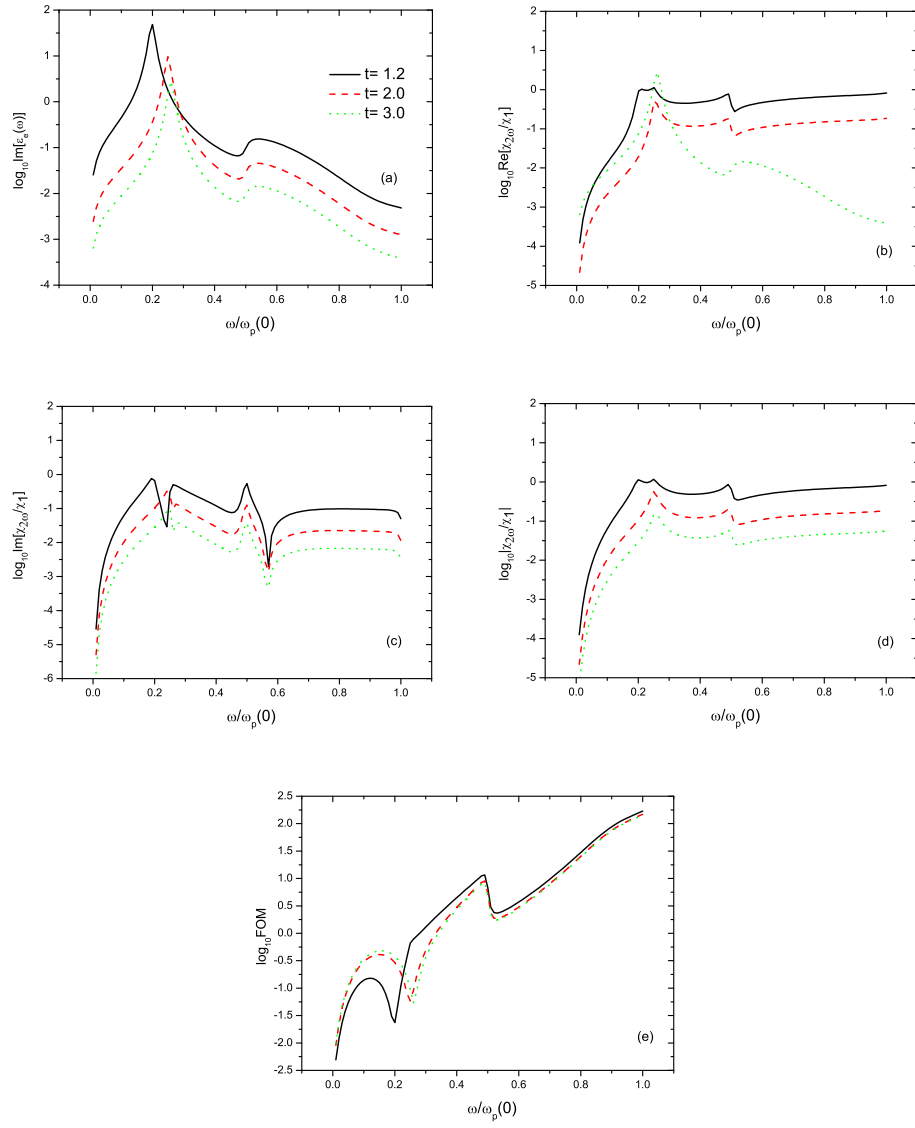


FIG. 4: /Jian, Fan, Huang, and Yu